

# Circumstellar disc of $\beta$ Pictoris: constraints on grain properties from polarization

N.V. Voshchinnikov<sup>1</sup> and E. Krügel<sup>2</sup>

<sup>1</sup> Sobolev Astronomical Institute, St. Petersburg University, Bibliotechnaya pl. 2, St. Petersburg-Peterhof, 198904 Russia

<sup>2</sup> Max-Planck-Institut für Radioastronomie, Auf dem Hügel 69, 53121 Bonn, Germany

Received 7 May 1999 / Accepted 14 September 1999

**Abstract.** We model the positional dependence of the optical polarization (BVRI-bands) in the circumstellar disc of  $\beta$  Pictoris as observed by Gledhill et al. (1991) and Wolstencroft et al. (1995). The particles are spherical, have a size distribution  $n(a) \sim a^{-q}$  and their number density decreases with distance from the star as  $r^{-s}$ . We consider both compact and porous grains. Varying the grain size and the exponent,  $s$ , of the density distribution as well as the refractive index of the grain material  $m$ , we find that the measured polarization, colours and brightness distribution in the disc are best reproduced by a model in which the grains are larger than interstellar grains (the minimum grain size  $a_{\min} = 0.15 \mu\text{m}$ ). The value of the maximum size is ill determined because it has little influence and was taken to be  $a_{\max} = 100 \mu\text{m}$ . The best-fit exponents of the power laws are  $q = 3.2$  and  $s = 3$ . The grains have in the R-band a refractive index  $m_R = 1.152 - 0.005i$ . Such a value is roughly appropriate for porous grains where half of the volume is ice and the other half vacuum, or where 24% of the volume consists of silicate and the remaining 76% of vacuum.

**Key words:** stars: individual:  $\beta$  Pic – stars: circumstellar matter – ISM: dust, extinction – polarization

## 1. Introduction

In the search for extrasolar planetary systems,  $\beta$  Pictoris and other Vega-type stars have become very popular and our present knowledge is summarized in several reviews (Backman & Paresce 1993; Vidal-Madjar & Ferlet 1994; Artymowicz 1994, 1996, 1997). In the last review, Artymowicz (1997) analyzed three principal components of the  $\beta$  Pictoris system: the star itself, the circumstellar dust and the circumstellar gas. Although there is an improved determination of the distance towards  $\beta$  Pic from the Hipparcos satellite (Crifo et al. 1997), the main conclusions of the previous analyses remain in force.

In general, information on dust comes from measurements of extinction, polarization, scattered light and thermal emission. For scattering, the geometrical relation between source,

scatterer and observer is essential. Whereas it is ill determined in reflection nebulae and allows only a very rough derivation of the grain properties, the geometrical configuration in the circumstellar disc of  $\beta$  Pic is clear and simple. In the case of  $\beta$  Pic one observes:

- i*) no circumstellar extinction (Crifo et al. 1997);
- ii*) very weak polarization of the star itself (Tinbergen 1979);
- iii*) scattered light from the nearly edge-on disc (Smith & Terrile 1984; Kalas & Jewitt 1995; Mouillet et al. 1997) and its polarization (Gledhill et al. 1991; Wolstencroft et al. 1995);
- iv*) an infrared excess (Aumann et al. 1984) which extends up to  $1300 \mu\text{m}$  (Chini et al. 1991); there are also mid IR images (Lagage & Pantin 1994; Pantin et al. 1997).

Many numerical calculations have been performed to explain the IR emission of  $\beta$  Pic (see detailed discussion in Li & Greenberg 1998). Depending on the wavelength range considered, the observations were reproduced using compact or fluffy grains with sizes ranging from smaller  $1 \mu\text{m}$  to up to 1 mm.

With respect to modelling the scattering and polarization of light from the disc of  $\beta$  Pic, Artymowicz et al. (1989), Kalas & Jewitt (1995, 1996) and Pantin et al. (1997) considered scattering only at one wavelength. They assumed either isotropic or anisotropic scattering without computing the asymmetry factor  $g$ . Scarrott et al. (1992), on the other hand, applied Mie theory and treated multi-wavelength scattering, however, the polarization was only calculated at the then available R-band. Artymowicz (1997) reproduced the observation in the V-band employing the empirical phase and polarization function of zodiacal and cometary dust.

In this paper, we model scattering and polarization at all observed wavelengths with particle cross sections computed from Mie theory. As a result, we are able to constrain the properties of the grains and to exclude certain choices of dust models which were hitherto thought possible.

## 2. Observations of polarization and colours

Imaging polarimetry of the  $\beta$  Pic disc was performed by Gledhill et al. (1991) in the R waveband and by Wolstencroft et al. (1995) in the B, V, R and I wavebands. The polarization patterns are centro-symmetric and indicate that  $\beta$  Pic itself is the illu-

---

Send offprint requests to: Nikolai V. Voshchinnikov  
(nvv@aispbu.spb.su)

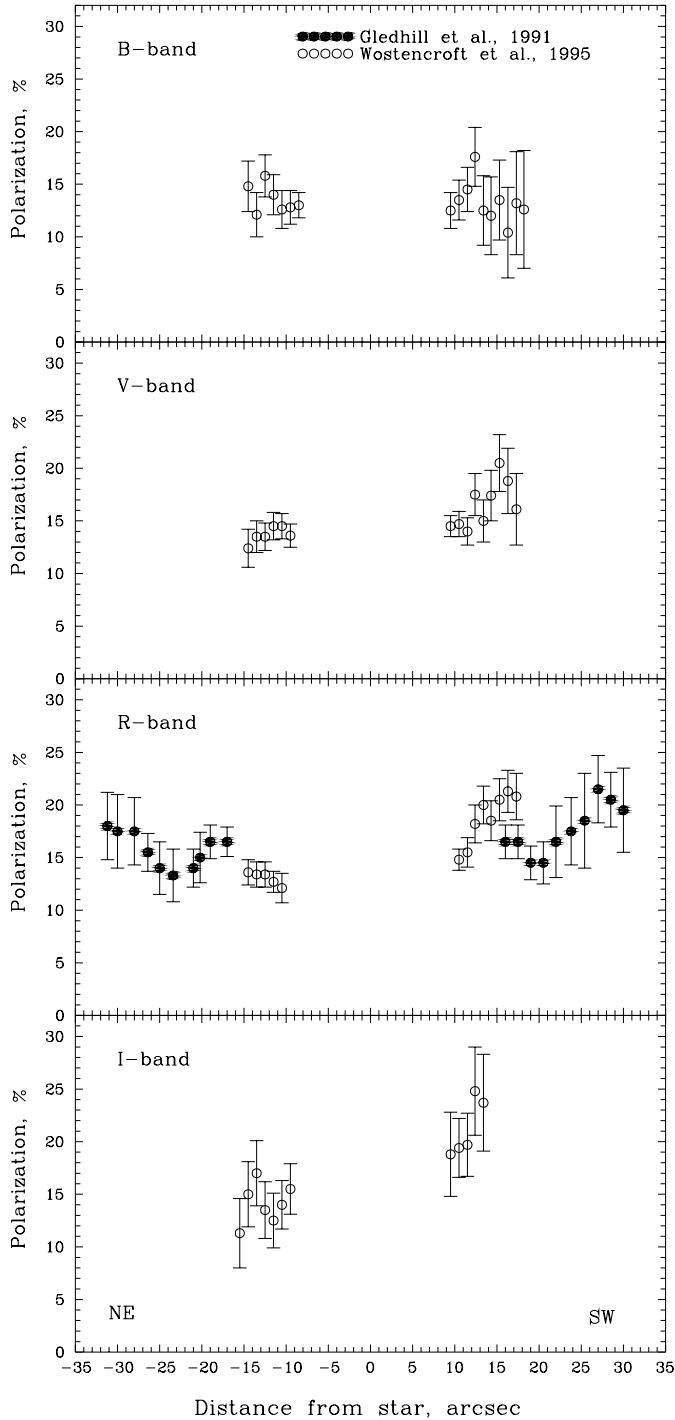


**Fig. 1.** Results of the multi-wavelength measurements of the polarization along the disc of  $\beta$  Pic.

minating source. The observational data are collected in Fig. 1 and suggest the asymmetry in the polarizing behaviour between the SW and NE sides, especially in the I-band.

The wavelength dependence of polarization  $P(\lambda)$  is typical of reflection nebulae and characterized by the increase of the polarization degree with wavelength. The increase is rather weak in the NE side and well pronounced in the SW side.

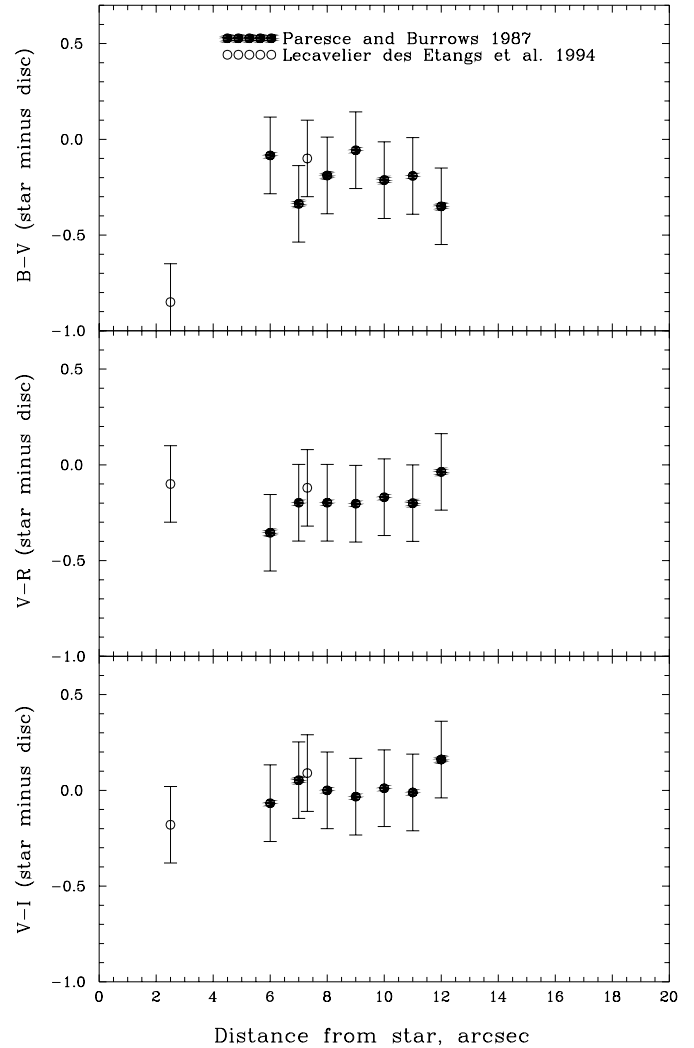


**Fig. 2.** Observed colours along the disc of  $\beta$  Pic.

The polarization vectors are oriented perpendicular to the disc (Gledhill et al. 1991; Wostencroft 1998). Tinbergen (1979) included  $\beta$  Pic in the list of zero polarization standard stars. Using a large diaphragm which included the disc he found that the mean degree of polarization over the wavelength range  $0.4\text{--}0.7\ \mu\text{m}$  is  $P = 0.020 \pm 0.008\%$ . This value is compatible with the absence of material in front of the star under the assumption of a maximum polarization efficiency ( $P/A_V = 3\%$ ) and implies  $A_V \simeq 0.006$  mag. The small polarization observed by Tinbergen (1979) should be due to dust scattering in the disc.

In ordinary reflection nebulae, the colour of the scattered light is usually bluer than the illuminating star at small offsets and redder at large distances (Voshchinnikov 1985). Unfortunately, the disc colours of  $\beta$  Pic were observed only out to  $\sim 12''$  offset (Paresce & Burrows 1987; Lecavelier des Etangs et al. 1993). The data of Fig. 2 indicate that the disc has the same colour as the star or is slightly redder. The colours do not depend on position, the only exception being the innermost point ( $\varphi = 2''.5$ ). It falls into the central gap which is presently the subject of various speculations.

We thus conclude that the properties of the scattered light are not peculiar. We therefore believe that the usual approach to the study of reflection nebulae can also be applied to  $\beta$  Pic.

### 3. Modelling

#### 3.1. Polarization mechanism and disc model

The variation of the position angle and the degree of polarization in the disc of  $\beta$  Pic speaks in favour of light scattering by spheres or arbitrarily oriented non-spherical particles. The disc is seen nearly edge-on. As it is optically thin, we can choose a model of single scattering in an optically thin medium. In this case, the radiation escaping from the disc at the angular distance  $\varphi$  from the star is the integral along the line of sight over some range of scattering angles ( $\Theta_1, 180^\circ - \Theta_1$ ), where

$$\Theta_1 = \arcsin\left(\frac{\varphi}{\varphi_{\max}}\right) \quad (1)$$

and  $\varphi_{\max}$  denotes the maximum angular size of the disc. We will adopt  $\varphi_{\max} = 45''0$  (Kalas & Jewitt 1995). With growing  $\varphi$ , the range of scattering angles, which is always centered at  $90^\circ$ , becomes narrower. A slightly tilted disc orientation ( $\sim 10^\circ$ ) would not change the picture of light scattering significantly.

#### 3.2. Step 1: Polarization diagrams vs scattering angle

As a first step in the modelling, we compute the polarization and scattered intensity of an elementary volume. In Mie scattering by spherical particles, such polarization at a given wavelength  $\lambda$  depends on the refractive index of the particle,  $m_\lambda = n_\lambda - k_\lambda i$ , and its radius  $a$ ,

$$P(m, a, \lambda, \Theta) = \frac{i_1(m, a, \lambda, \Theta) - i_2(m, a, \lambda, \Theta)}{i_1(m, a, \lambda, \Theta) + i_2(m, a, \lambda, \Theta)}. \quad (2)$$

Here  $i_1$  and  $i_2$  are the dimensionless intensities which determine the radiation scattered perpendicular and parallel to the scattering plane, respectively (van de Hulst 1957; Bohren & Huffman 1983).

Fig. 3 shows the polarization diagrams at  $\lambda = 0.70 \mu\text{m}$  (R-band) for which the observational database is largest (Fig. 1). The particles considered are a mixture of silicate and ice. They could be porous, i.e. contain some volume fraction of vacuum. Porous grains have been discussed many times for the disc of  $\beta$  Pic (see Artymowicz 1997; Li & Greenberg 1998). The refractive indices used are specified in Table 1. Note that we chose the volume fractions of the grain constituents in such a way that several of the refractive indices in Table 1 are identical, although they refer to grains of different chemical composition. The cross sections of grains with a silicate core and an ice mantle were computed from Güttler's (1952) theory for two-layered spheres.

It is important to note that all polarization diagrams of Fig. 3 are similar and independent of the particle composition and structure. Small grains belong to the Rayleigh domain where the polarization has the well known bell-like shape with the maximum at  $\Theta = 90^\circ$ . Polarization diagrams for very large

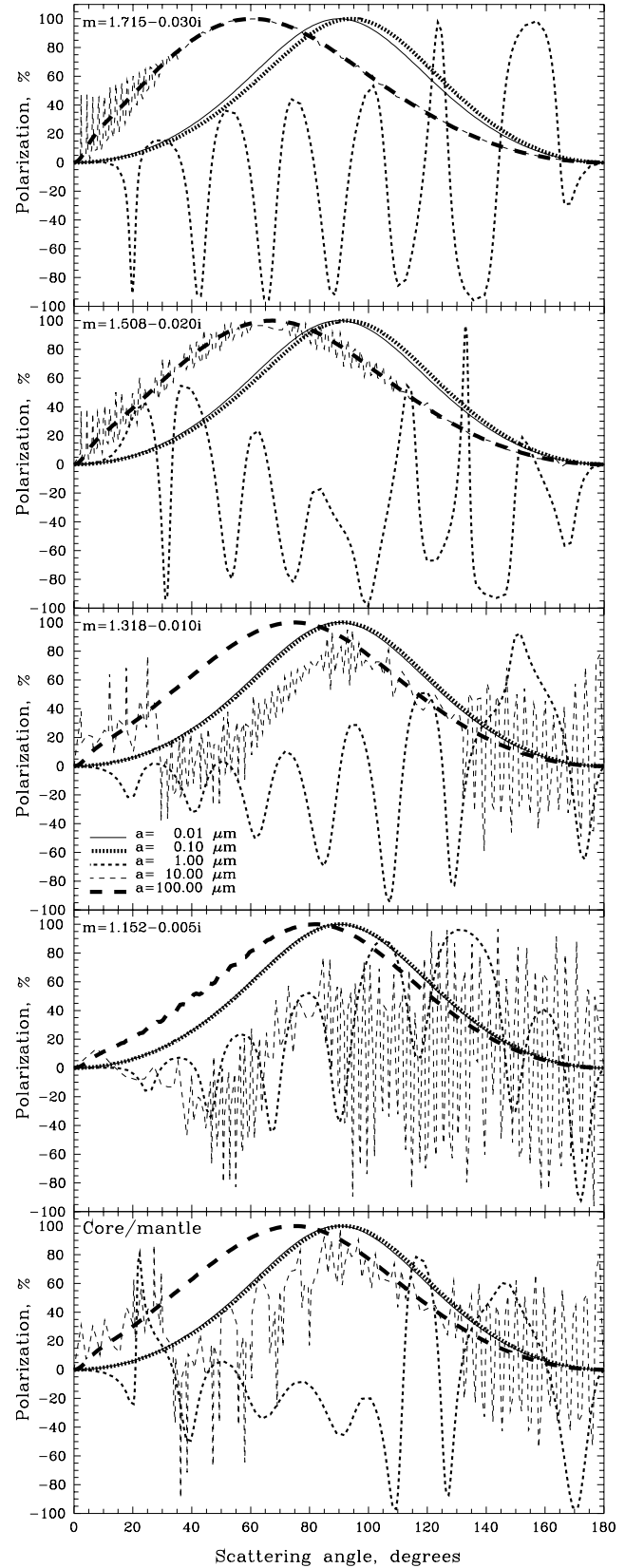


**Fig. 3.** The degree of linear polarization for various kinds of particles. Their composition and refractive indices are given in Table 1. The peak of the curve for  $a = 0.1 \mu\text{m}$  is always slightly shifted to larger values of scattering angle relative to those for  $a = 0.01 \mu\text{m}$ .

**Table 1.** Grain refractive indices  $m_R$  at  $\lambda = 0.70 \mu\text{m}$ 

Refractive index	Particle composition
$1.715 - 0.030i$	compact silicate grains
$1.508 - 0.020i$	{ composite grains: mixture of 50% silicate + 50% ice porous grains: mixture of 72% silicate + 28% vacuum
$1.310 - 0.010i$	{ compact grains of dirty ice porous grains: mixture of 45% silicate + 55% vacuum
$1.152 - 0.005i$	{ porous grains: mixture of 50% ice + 50% vacuum porous grains: mixture of 24% silicate + 76% vacuum
$1.715 - 0.030i/1.310 - 0.010i$	core–mantle grains: silicate core + ice mantle

Optical constants for silicate are from Draine (1985), for dirty ice from Greenberg (1968).

The optical constants for composite and porous grains were obtained from the Bruggeman rule (Bohren & Huffman 1983).

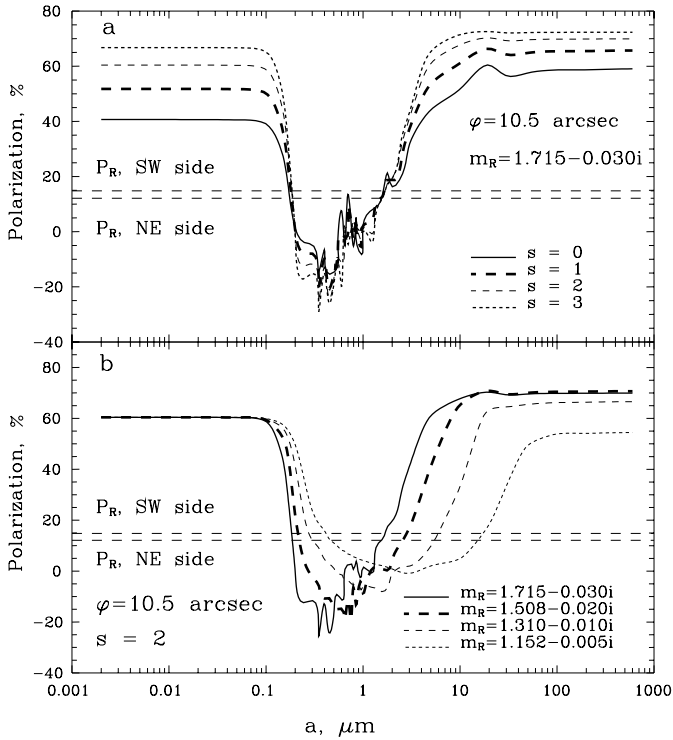


**Fig. 4.** **a** Upper panel: polarization vs particle size at the angular distance  $\varphi = 10''.5$  for various exponents,  $s$ , of the dust density distribution. The grains are compact silicates with  $m_R$  as indicated. The horizontal dashed lines show the observed polarization  $P_R$  in the NE and SW sides. **b** Lower panel: as **a**, but now for a fixed density distribution ( $s = 2$ ) and particles of various refractive indices.

spheres are also simple. They resemble smooth curves with the maximum at  $\Theta \approx 70^\circ$ . In both cases, the polarization does not change sign and reaches  $\sim 100\%$ . For particles of intermediate size, polarization reverses sign repeatedly and a ripple-like structure is seen.

This behaviour of the curves  $P(\lambda)$  in Fig. 3 reflects the general principles of light scattering by small particles and does not principally change for non-spherical bodies, like spheroids, cylinders, bispheres, or fluffy aggregates arbitrarily aligned in space (Mishchenko et al. 1996; Kolokolova et al. 1997; Lumme

et al. 1997). Moreover, Lumme et al. (1997) demonstrated that Mie theory of spheres reproduces the polarization diagrams for complex particles rather well, except sometimes for forward and backward scattering.

The polarization measurements in  $\beta$  Pic were made at off-sets from  $\varphi = 8''.5$  to  $31''.2$  (see Fig. 1). According to Eq. (1), the scattering angles vary in the limits from  $(11^\circ - 169^\circ)$  to  $(44^\circ - 136^\circ)$ . With these limits, we conclude with the aid of Fig. 3: *the polarimetric observations of  $\beta$  Pic cannot be explained by light scattering of very small ( $< 0.1 \mu\text{m}$ ) or very large ( $> 10 \mu\text{m}$ ) particles only because they produce the polarization too high for the scattering angle range.*

### 3.3. Step 2: Polarization diagrams vs particle size

As the second step of the modelling procedure we include averaging along the line of sight (scattering angles) at fixed angular distance  $\varphi$ . We adopt that the number density of dust grains in the disc has a power-law distribution

$$n_d(r) = \begin{cases} 0, & r < r_0, \\ n_0 \left(\frac{r}{r_0}\right)^{-s}, & r_0 \leq r < r_{\text{out}}. \end{cases} \quad (3)$$

Here,  $r_0$  is the radius of the central hole where the density is equal to  $n_0$  and  $r_{\text{out}}$  is the outer radius of the disc. The latter is given by  $r_{\text{out}} = D\varphi_{\text{max}} = 19.28 \cdot 45 \approx 870$  AU, assuming a distance  $D = 19.28$  pc (Crifo et al. 1997). The central cavity reaches out to  $\varphi \lesssim \varphi_0 \approx 6''.0$  (Artymowicz et al. 1989).<sup>1</sup> With these numbers,  $r_0 \approx 120$  AU and the ratio of the inner to outer radius equals  $\varphi_0/\varphi_{\text{max}} = r_0/r_{\text{out}} \approx 0.13$ .

The polarization degree can be expressed as

$$P(m, a, \lambda, \varphi, s) = \frac{\langle I_1 \rangle - \langle I_2 \rangle}{\langle I_1 \rangle + \langle I_2 \rangle}, \quad (4)$$

$$\langle I_j \rangle = \frac{\mathcal{K}}{\varphi^{s+1}} \int_{\Theta_1}^{\pi - \Theta_1} i_j(m, a, \lambda, \Theta) \sin^s \Theta \, d\Theta, \quad (5)$$

<sup>1</sup> The adaptive optics observations made by Mouillet et al. (1997) show that the scattered light is present at angular distances up to  $\varphi \approx 1''.5$ . Perhaps, this is the light from the outer disc scattered in almost forward and backward directions. However, because the polarization observations are made outside of this radius, this does not impact on the result, given in the single scattering case.

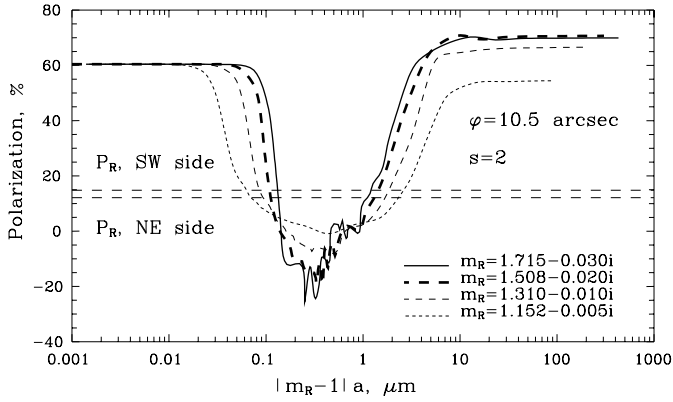


**Fig. 5.** As Fig. 4b, but with polarization plotted vs the parameter  $|m_R - 1|a$ .

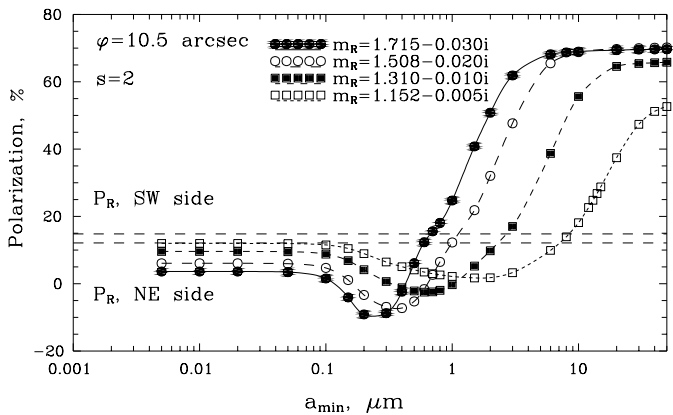


**Fig. 6.** Polarization vs  $a_{\min}$  at the angular distance  $\varphi = 10''.5$ . The upper size limit equals  $a_{\max} = 100 \mu\text{m}$  and the exponent of the size distribution  $q = 3.5$ .

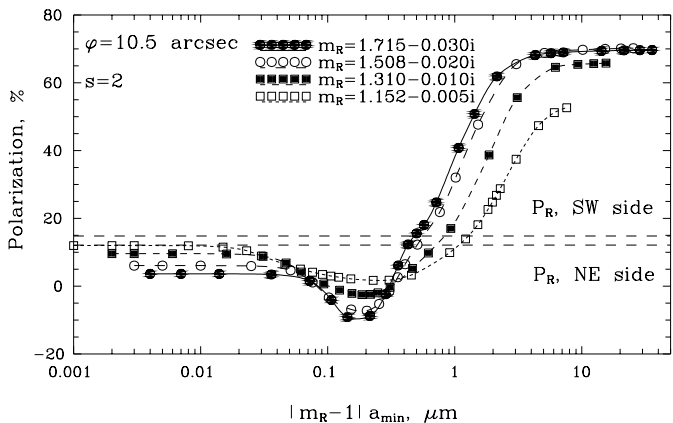


**Fig. 7.** As Fig. 6, but with polarization vs the parameter  $|m_R - 1|a_{\min}$ .

where the intensities  $I_j$  ( $j = 1, 2$ ) depend on  $m$ ,  $a$ ,  $\lambda$ ,  $\varphi$ ,  $s$ , and  $\mathcal{K}$  is a constant. If  $\varphi < 6''.0$  and  $\sin \Theta > \frac{1}{0.13} \cdot \frac{\varphi}{\varphi_{\max}}$ , the line of sight intersects the hole.

Examples of polarization diagrams are shown in Fig. 4 at the offset  $\varphi = 10''.5$  for different types of particles and various values of  $s$ . The polarization degree observed in the R-band at this offset angle in the NE and SW extensions is shown by horizon-

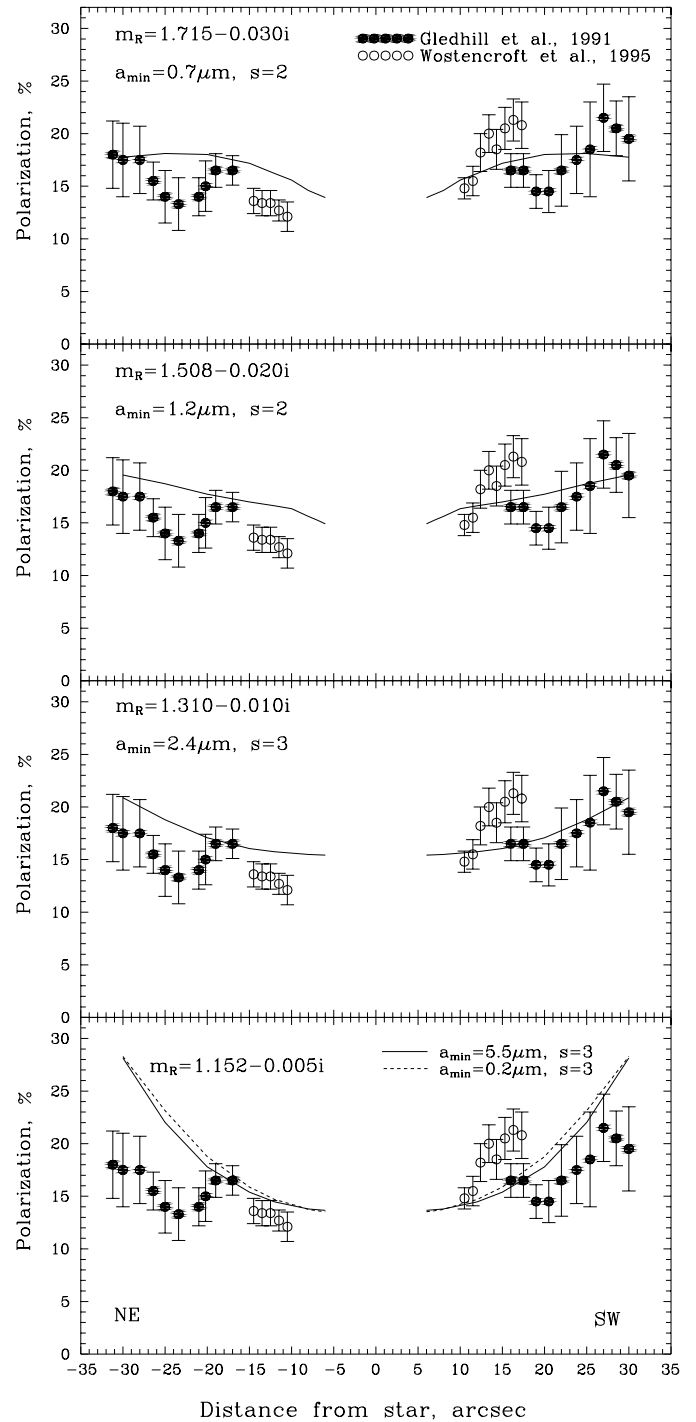


**Fig. 8.** Polarization in the disc of  $\beta$  Pic as a function of the angular offset for the R-band. Solid lines present models with different refractive indices (see Table 1). In all calculations,  $a_{\max} = 100 \mu\text{m}$  and  $q = 3.5$ . The other model parameters ( $a_{\min}$  and  $s$ ) are shown in the panels.

tal dashed lines. From this figure we again conclude that grains of intermediate size have to be included into consideration to explain the observed polarization. Interestingly, the polarization observed at given offset may be explained for any density distribution of particles: as evident from Fig. 4a (the parameter

**Table 2.** Observational and theoretical colour excesses in the disc of  $\beta$  Pic at  $\varphi = 10''5$ .

Colour excess	Observations	Model 1	Model 2	Model 3	Model 4	Model 5
$(B-V)_{\star\text{-disc}}$	$-0^m21 \pm 0^m20$	$-0^m217$	$-0^m213$	$-0^m221$	$-0^m228$	$0^m034$
$(V-R)_{\star\text{-disc}}$	$-0^m17 \pm 0^m20$	$-0^m200$	$-0^m226$	$-0^m228$	$-0^m252$	$0^m061$
$(V-I)_{\star\text{-disc}}$	$0^m01 \pm 0^m20$	$-0^m313$	$-0^m344$	$-0^m354$	$-0^m400$	$0^m105$

Model 1:  $m_R = 1.715 - 0.030i$ ,  $a_{\min} = 0.7 \mu\text{m}$ ,  $s = 2$  ( $\gamma = 3.4$ ,  $\Lambda = 0.67$ ,  $g = 0.80$ ).

Model 2:  $m_R = 1.508 - 0.020i$ ,  $a_{\min} = 1.2 \mu\text{m}$ ,  $s = 2$  ( $\gamma = 3.4$ ,  $\Lambda = 0.66$ ,  $g = 0.86$ ).

Model 3:  $m_R = 1.310 - 0.010i$ ,  $a_{\min} = 2.4 \mu\text{m}$ ,  $s = 3$  ( $\gamma = 4.2$ ,  $\Lambda = 0.67$ ,  $g = 0.91$ ).

Model 4:  $m_R = 1.152 - 0.005i$ ,  $a_{\min} = 5.5 \mu\text{m}$ ,  $s = 3$  ( $\gamma = 4.4$ ,  $\Lambda = 0.67$ ,  $g = 0.96$ ).

Model 5:  $m_R = 1.152 - 0.005i$ ,  $a_{\min} = 0.2 \mu\text{m}$ ,  $s = 3$  ( $\gamma = 4.4$ ,  $\Lambda = 0.89$ ,  $g = 0.82$ ).

All models have  $a_{\max} = 100 \mu\text{m}$  and  $q = 3.5$ .

$\gamma$  – exponent in the brightness distribution,  $\Lambda$  – single scattering albedo,  $g$  – asymmetry factor.

$s$  determines only the polarization level at low and large size limits).

The curves plotted in Fig. 4b look even more similar if we use the product  $|m - 1|a$  as an argument. That this is so is well known for the extinction efficiency (e.g. Greenberg 1968). The corresponding polarization diagrams are shown in Fig. 5. Thus, considering light scattering in the continuum, the effects of refractive index and particle size cannot be separated. In other words, *we can only estimate  $|m - 1|a$ , the product of refractive index times particle size, from observations at one wavelength*. In more realistic models, we must also average over the size distribution  $n_d(a)$ . Afterwards the spikes in polarization seen in Fig. 3 disappear. We use the power-law

$$n_d(a) \sim a^{-q} \quad (6)$$

with minimum and maximum radii  $a_{\min}$  and  $a_{\max}$ , respectively. Figs. 6 and 7 are analogous to Fig. 4 and 5, but include an average over the size distribution. The upper radius and the exponent are kept fixed ( $a_{\max} = 100 \mu\text{m}$ ,  $q = 3.5$ ) and  $a_{\min}$  is being varied.

The changes of  $a_{\min}$  are most important with respect to polarization. The increase or decrease of the maximum size has no influence if  $|m - 1|a_{\max} \gtrsim 10$ . So if very large particles are present in the disc of  $\beta$  Pic, they are not visible as scatterers at waveband R. Changes in  $q$  do not affect the overall picture and will be discussed in Sect. 3.6. Figs. 6 and 7 contain plots for all refractive indices listed in Table 1. The figures show that *in order to explain the observed polarization one needs to keep  $a_{\min}$  in the range  $0.6 \mu\text{m} \lesssim a_{\min} \lesssim 10 \mu\text{m}$* . However, very porous grains with small values of  $a_{\min}$  may, in principle, be used to model the observations as well.

### 3.4. Step 3: Polarization vs angular distance from star

In the next step, we model the angular distribution of polarization using the minimum cut-off in the size distribution as estimated from Fig. 6. The curves in Fig. 8 demonstrate that the same observations may be satisfactorily fit with particles of different composition by changing only the parameters  $a_{\min}$  and  $s$ .<sup>2</sup> Note that the variations of  $s$  and  $a_{\min}$  influence the polar-

<sup>2</sup> Actually, the choice of the parameter  $s$  is determined by the radial brightness distribution of the scattered light,  $I(\varphi)$ . For the outer parts

of the disc of  $\beta$  Pic ( $\varphi > 6''0$ ),  $I(\varphi) \propto \varphi^{-\gamma}$  with  $\gamma = 3.6\text{--}4.3$  (Kalas & Jewitt 1995). The values of  $\gamma$  for the models considered are given in Table 2.

ization mainly at small and large offset angles. (We adopted  $a_{\max} = 100 \mu\text{m}$  and  $q = 3.5$ .) Therefore, *the polarimetric observations of the extended sources (nebulae, circumstellar shells, galaxies) at one wavelength do not allow to determine the chemical composition of particles*. Numerous other sets of refractive indices and size parameters may also explain the observations. As an example, let us consider the model of Scarrott et al. (1992). They reproduced the angular dependence of the scattered light and polarization in the R-band observed by Gledhill et al. (1991) with silicate particles of  $m_R = 1.65 - 0.05i$  and  $a_{\min} = 0.01 \mu\text{m}$ ,  $a_{\max} = 3 \mu\text{m}$ ,  $q = 4.0$ ,  $s = 2.75$ . However, the disc colours in their model are too red compared to those observed (from  $-0^m72$  in  $(B-V)_{\star\text{-disc}}$  to  $-1^m24$  in  $(V-I)_{\star\text{-disc}}$ ).

### 3.5. Step 4: Polarization vs wavelength

With the parameters found from modelling of the polarization in the R-band (see Fig. 8), we calculated the wavelength dependence of polarization at the offset distance  $\varphi = 10''5$ . We also checked the colour excesses given by the corresponding model (see Table 2) and compared them with observations.

The results are shown in Fig. 9 and Table 2. It is clear that despite our thorough procedure and the successful fits of the changes in polarization and brightness in the R-band with angle  $\varphi$  (see Fig. 8 and Table 2), the dependence  $P(\lambda)$  cannot be well explained for any refractive index. From Table 2 it also follows that the colour index V-I is crucial for the choice of the model. The colours in the models 1 – 4 are too red and these models must be rejected. In principle, the correct polarization behaviour (i.e. its growth with wavelength) can be reproduced for all refractive indices of Table 1 if the minimum size  $a_{\min}$  is lowered. But even if we were to fit the dependence  $P(\lambda)$ , very small particles would yield unacceptably blue colours.

*So in order to explain all colour and polarization observations we need to reduce the lower limit of the size distribution,  $a_{\min}$ , and the refractive index  $m$ .*

of the disc of  $\beta$  Pic ( $\varphi > 6''0$ ),  $I(\varphi) \propto \varphi^{-\gamma}$  with  $\gamma = 3.6\text{--}4.3$  (Kalas & Jewitt 1995). The values of  $\gamma$  for the models considered are given in Table 2.

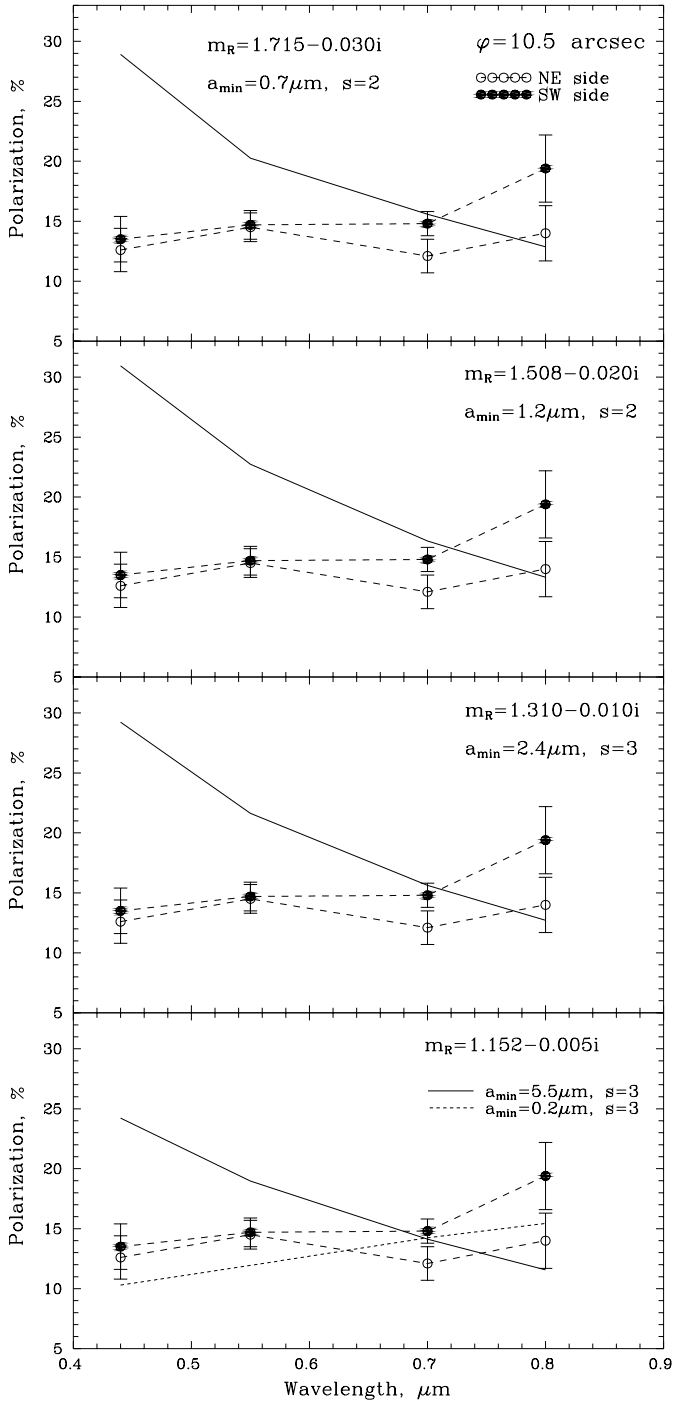


**Fig. 9.** The wavelength dependence of polarization in the disc of  $\beta$  Pic at the angular distance  $\varphi = 10''.5$ . The observations in the SW and NE sides and their errors are plotted by dashed lines. The parameters of the model are the same as in Fig. 8.

### 3.6. Step 5: Polarization and colours: Whole picture

Finally, we suggest a fit to the angular dependence of the polarization (in all wavebands) and the colour excesses (see Figs. 10 and 11). In order to improve the fits, we varied the parameters  $a_{\min}$  and  $q$  around the values given in Table 2 for model 5. Un-

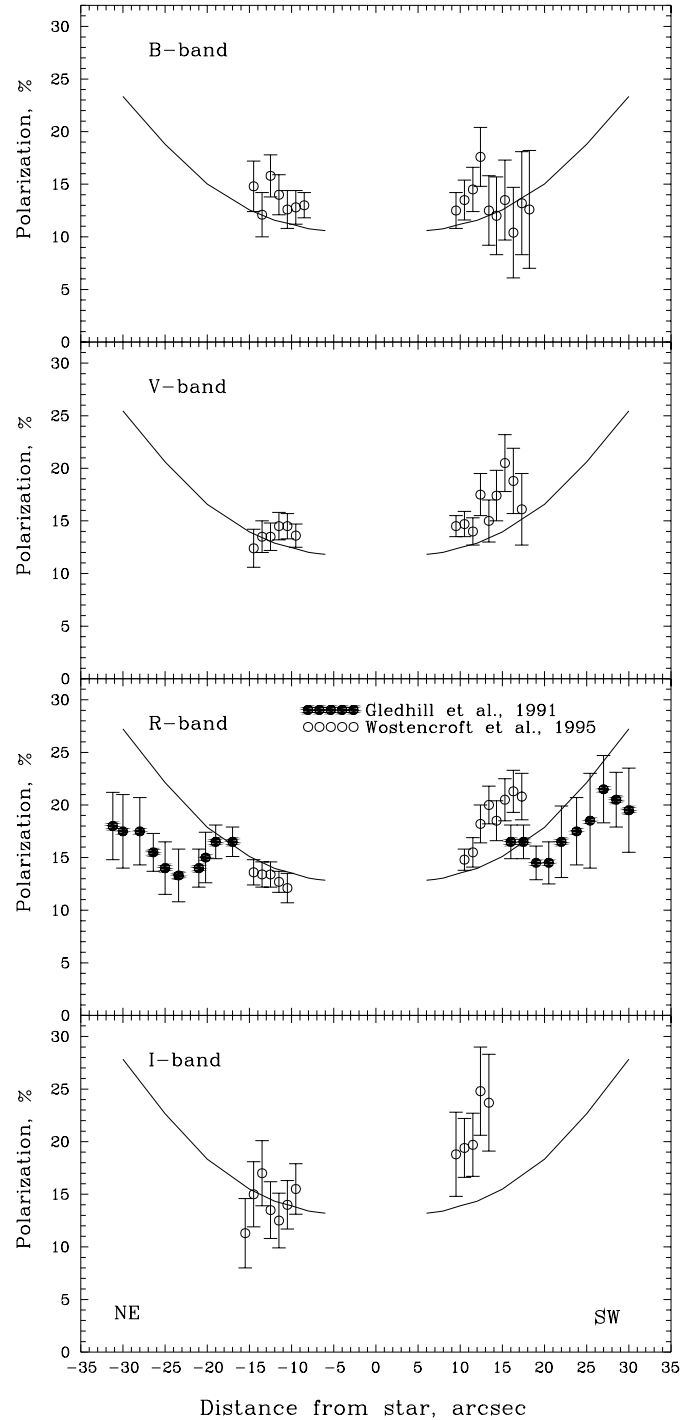


**Fig. 10.** The polarization observed in the disc of  $\beta$  Pic. The solid lines correspond to the theoretical models for which  $m_R = 1.152 - 0.005i$ ,  $a_{\min} = 0.15 \mu\text{m}$ ,  $a_{\max} = 100 \mu\text{m}$ ,  $q = 3.2$  and  $s = 3$ .

fortunately, there remains some problem for the position with the minimum distance  $\varphi = 2''.5$ . The colour index B–V can be modeled only if the grains have very narrow size distribution around  $a \sim 15 \mu\text{m}$ , but with such grains the polarization at observed offsets becomes too large (see Fig. 4).

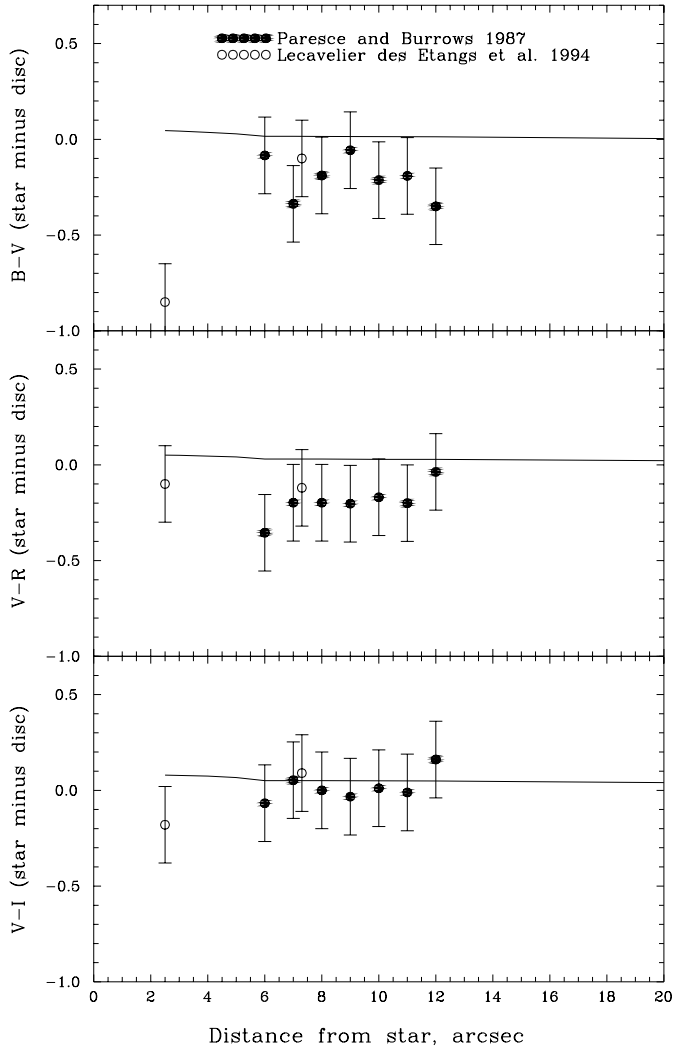


**Fig. 11.** The colour excesses observed in the disc of  $\beta$  Pic. The theoretical model has the same parameters as in Fig. 10.

#### 4. Concluding remarks

All models presented here were constructed with a small number of parameters which are rather well determined. Our favourite model presented in Figs. 10, 11 has parameters:

$$\begin{aligned} m_R &= 1.152 - 0.005i, \\ a_{\min} &= 0.15 \mu\text{m}, \\ a_{\max} &= 100 \mu\text{m}, \\ q &= 3.2, \\ s &= 3. \end{aligned}$$

The model fits reasonably well the observed angular dependence of polarization (in four wavebands), three colour excesses and the radial brightness distribution. The calculated values of the exponent in the brightness distribution, single scattering albedo and asymmetry factor in the R-band are:

$$\begin{aligned} \gamma &= 4.4, \\ \Lambda &= 0.88, \end{aligned}$$

$$g = 0.79.$$

Still better fits could be obtained assuming different dust properties on either side of the disc. Previous estimates of the grain albedo in the disc of  $\beta$  Pic based on visible/IR models gave  $\Lambda = 0.5 \pm 0.2$  (Artymowicz 1997), which is smaller than our value for very porous grains. But Artymowicz et al. (1989) also derived  $\Lambda \simeq 0.9$ .

As usual, the albedo  $\Lambda$  of the grains was estimated independently of the scattering phase function. Evidently, the latter cannot be isotropic in the visual because so far all suggested grain sizes imply forward scattering. The value of our model ( $g \approx 0.8$ ) is larger than previous ones. Using the Heyney–Greenstein phase function, Kalas & Jewitt (1995) found that the brightness distribution observed in the disc of  $\beta$  Pic in the R-band may be reproduced with  $0.3 \leq |g| \leq 0.5$ . Note that mirror particles (with  $g < 0$ ) used by Kalas & Jewitt (1995, 1996) are astronomical nonsense because no grain material (with the exception of very small iron particles) gives at visual wavelengths a negative asymmetry parameter. Even pure conductors ( $m = \infty$ ) have  $g \approx -0.2$  only (van de Hulst 1957).

In our favourite model (see Figs. 10, 11) we only specify the refractive index (see Table 1). It was taken arbitrarily and is not motivated from the physical point of view. From other side, the porous particles may be easily kept in the shell because the radiation pressure acting on them is smaller: we found that for silicate grains of radii  $a \gtrsim 2.0 \mu\text{m}$  with 76% porosity (Table 1) the radiation pressure force is smaller than gravitational force.

Very porous aggregates were adopted by Li & Greenberg (1998) to explain the IR observations. Mie theory can, of course, not be applied in such cases. Although Li & Greenberg used a standard mixing rule to treat the fluffy aggregates, the underlying theory has not been developed for particles with sizes larger than the wavelength nor for computing the scattering of light.

We modeled scattering and polarization in the disc of  $\beta$  Pic at all wavelengths where it has been observed. Because the properties of the scattered light are not peculiar, we could compute particle cross sections from Mie theory. Our models exclude the possibility that the grains are compact spheres, or that they are all very small or all very large grains. Instead, the particles must be rather porous (degree of porosity  $\gtrsim 50\%$ ) and have a lower cut-off in the size distribution as small as  $a_{\min} \sim 0.2 \mu\text{m}$ . This limit is larger than the mean size of interstellar grains. Our model can be further verified by computing the resulting IR fluxes and check how well they agree with observations.

*Acknowledgements.* The authors are thankful to Vladimir Il'in, Nicolas Mauron and an anonymous referee for helpful comments. NVV wishes to thank for hospitality Max–Planck–Institut für Radioastronomie where this work was begun. The work was partly supported by grants of the program “Astronomy” of the government of the Russian Federation, the program “Universities of Russia – Fundamental Researches” (grant N 2154) and the Volkswagen Foundation.

## References

- Artymowicz P., 1994, In: Ferlet R., Vidal–Madjar A. (eds.) Circumstellar dust disks and planet formation. p. 47
- Artymowicz P., 1996, In: Käufel H.U., Siebenmorgen R., (eds.) The role of dust in the formation of stars. p. 137
- Artymowicz P., 1997, *Annu. Rev. Earth Planet. Sci.* 25, 175
- Artymowicz P., Burrows C., Paresce F., 1989, *ApJ* 337, 494
- Aumann H.H., Beichman C.A., Gillet F.C., et al., 1984, *ApJ* 278, L23
- Backman D.E., Paresce F., 1993, In: Levy E.E., et al. (eds.) *Protostars and Planets III*, p. 1253
- Bohren C.F., Huffman D.R., 1983, *Absorption and scattering of light by small particles*. John Wiley, New York
- Chini R., Krügel E., Shustov B., Tutukov A., Kreysa E., 1991, *A&A* 252, 220
- Crifo F., Vidal–Madjar A., Lallement R., Ferlet R., Gerbaldi M., 1997, *A&A* 320, L29
- Draine B.T., 1985, *ApJS* 57, 587
- Greenberg J.M., 1968, In: Middlehurst B.M., Aller L.H. (eds.) *Stars and stellar systems*. Vol. VII, Uni. Chicago Press, p. 221
- Gledhill T.M., Scarrott S.M., Wolstencroft R.M., 1991, *MNRAS* 252, 50p
- Güttler A., 1952, *Ann. Phys.* 6, Bd. 11, 65
- Kalas P., Jewitt D., 1995, *AJ* 110, 794
- Kalas P., Jewitt D., 1996, *AJ* 111, 1347
- Kolokolova L., Jockers K., Chernova G., Kiselev N., 1997, *Icarus* 126, 351
- Lagage P.O., Pantin E., 1994, *Nat* 369, 628
- Lecavelier des Etangs A., Perrin G., Ferlet R., et al., 1993, *A&A* 274, 877
- Li A., Greenberg J.M., 1998, *A&A* 331, 291
- Lumme K., Rahola J., Hovenier J.W., 1997, *Icarus* 126, 455
- Mishchenko M.I., Travis L.D., Mackowski D.W., 1996, *JQSRT* 55, 535
- Mouillet D., Lagrange A.M., Beuzit J.L., Renaud N., 1997, *A&A* 324, 1083
- Pantin E., Lagage P.O., Artymowicz P., 1997, *A&A* 327, 1123
- Paresce F., Burrows C., 1987, *ApJ* 319, L23
- Scarrott S.M., Draper P.W., Gledhill T.M., 1992, In: Gondhalekar P.M. (ed.) *Dusty discs*. p. 8
- Smith B.A., Terrile R.J., 1984, *Sci* 226, 1421
- Tinbergen J., 1979, *A&AS* 35, 325
- Vidal–Madjar A., Ferlet R., 1994, In: Ferlet R., Vidal–Madjar A. (eds.) *Circumstellar dust disks and planet formation*. p. 7
- van de Hulst H.C., 1957, *Light scattering by small particles*. John Wiley, New York
- Voshchinnikov N.V., 1985, In: Morozhenko A.V. (ed.) *Photometric and polarimetric investigations of the celestial bodies*. Kiev, p. 111
- Wolstencroft R.M., 1998, private communication
- Wolstencroft R.M., Scarrott S.M., Gledhill T.M., 1995, *Ap&SS* 224, 395